

Fault reactivation and propagation during the 2017 Pohang earthquake sequence



Jin-Han Ree^{a,*}, Kwang-Hee Kim^b, Hobin Lim^c, Wooseok Seo^b, Sungshil Kim^d, Xiangyi An^a, YoungHee Kim^c

^a Department of Earth and Environmental Sciences, Korea University, Seoul, 02841, Republic of Korea

^b Department of Geological Science, Pusan National University, Busan, 46241, Republic of Korea

^c School of Earth and Environmental Sciences, Seoul National University, Seoul, 08826, Republic of Korea

^d Department of Earth Science Education, Chonnam National University, Gwangju, 61186, Republic of Korea

ARTICLE INFO

Keywords:

2017 Pohang earthquake
Fluid injection
Enhanced geothermal system
Slip tendency
Fault reactivation

ABSTRACT

A commission of the Korean government on the 2017 M_w 5.5 Pohang earthquake concluded that seismic activity was triggered by fluid injection from the nearby Pohang enhanced geothermal system. The temporal and spatial distribution of hypocenters (depth range of 3–6 km) was recorded by our local seismic array for 345 days. It included, in addition to the mainshock, 10 foreshocks and 3090 aftershocks, indicating a complex geometry of propagating rupture segments, including the main segment and four subsidiary segments (SS1 to SS4). The fault kinematics of the earthquake sequence were dominated by strike and reverse slips. The aftershock sequence showed a decrease in frequency during the first 83 days after the mainshock, in accordance with Omori's law. This was followed by a sudden surge in aftershock frequency associated with the M_L 4.6 event (11 February 2018), and another decay following Omori's law. The aftershock surge of the M_L 4.6 event corresponds to the development of SS4. A calculation of the Coulomb stress change caused by the mainshock shows that a significant increase in stress occurred around SS4, thus suggesting that rupture along this segment was triggered by the mainshock. With respect to the current stress field, all rupture planes apart from that of SS4 are optimally oriented for reactivation, highlighting the potential risk associated with fluid injection into this fault.

1. Introduction

Fluid injection from an enhanced geothermal system (EGS) has been suggested as the cause of the 2017 M_L 5.4 (M_w 5.5) Pohang earthquake (Kim et al., 2018a; Grigoli et al., 2018). A report by the Overseas Research Advisory Committee on the Pohang earthquake concluded that the earthquake was triggered by anthropogenic activity associated with the EGS (Korean Government Commission, 2019; Lee et al., 2019; Ellsworth et al., 2019). This earthquake was the second largest and most damaging instrumental earthquake in South Korea. It differed from previous earthquakes in two different aspects. First, the focal depth of the Pohang earthquake sequence (4–6 km; Kim et al., 2018a) was shallower than that of other inland earthquakes in Korea (mostly 10–20 km; Kim et al., 2016; Korea Meteorological Administration earthquake data service, <http://www.weather.go.kr/weather/earthquake/volcano/domesticlist.jsp>). Second, the earthquake occurred in a relatively quiet area of Pohang in seismic terms (Kim et al., 2018a). For example,

the epicenter of the 2016 M_L 5.8 Gyeongju earthquake (Kim et al., 2016), the largest instrumental earthquake in South Korea, occurred in an area where many historical earthquakes have been recorded, including the 1997 M_L 4.3 Gyeongju earthquake (Chung and Kim, 2000). Few historical earthquakes have been recorded from the area around the Pohang EGS site (Lee et al., 1986), although the epicentral location of the historical earthquakes is somewhat inaccurate.

Foreshocks, mainshock, and aftershocks were recorded by temporary seismic stations in the area of the Pohang EGS site (<3 km), which were deployed five days before the 2017 Pohang earthquake (Kim et al., 2018a). Using these data, we examined the geometry and evolution of rupture planes during the Pohang earthquake sequence. The aims of this paper are to characterize the rupture process and to understand the potential or tendency of rupture planes to slip (Morris et al., 1996; Collettini and Trippetta, 2007). The potential reactivation of rupture planes that are misoriented with respect to the current stress field is also discussed.

* Corresponding author.

E-mail address: reejh@korea.ac.kr (J.-H. Ree).

<https://doi.org/10.1016/j.geothermics.2021.102048>

Received 20 February 2020; Received in revised form 26 August 2020; Accepted 18 January 2021

Available online 30 January 2021

0375-6505/© 2021 The Author(s). Published by Elsevier Ltd. This is an open access article under the CC BY-NC-ND license

(<http://creativecommons.org/licenses/by-nc-nd/4.0/>).

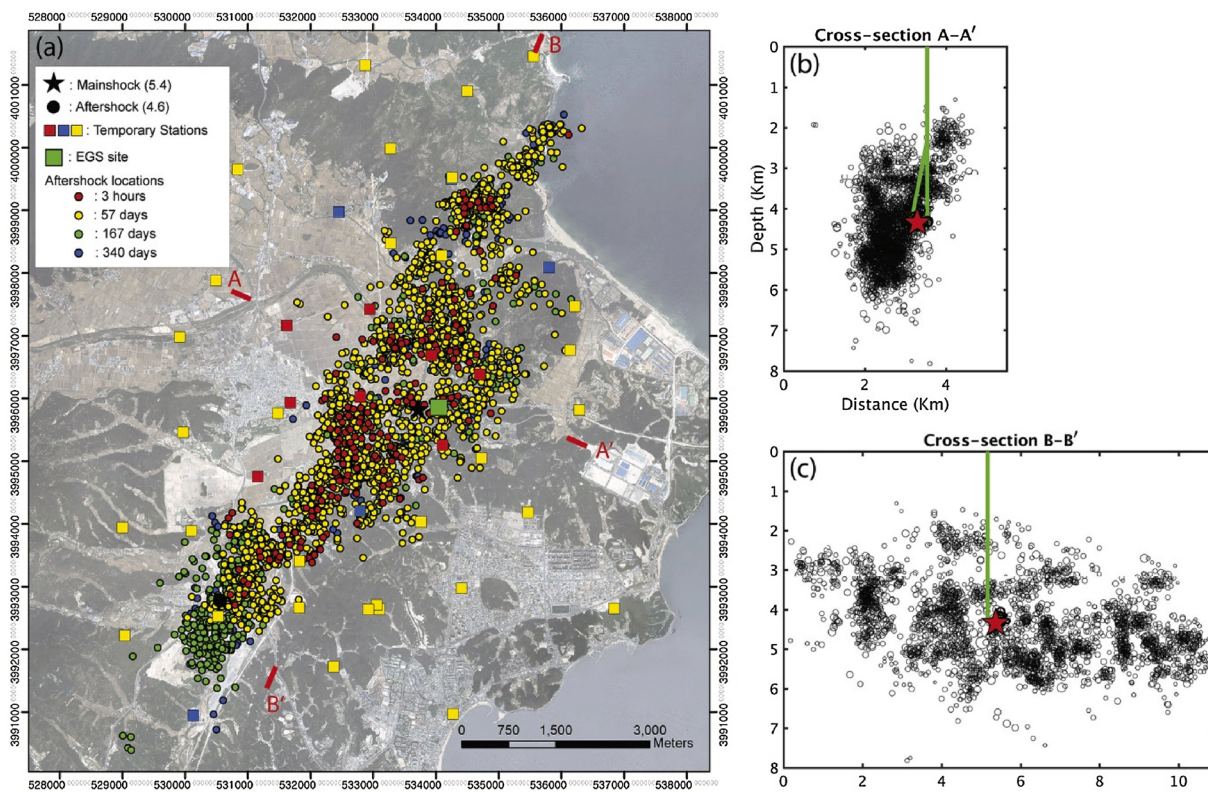


Fig. 1. Map of epicenters and cross-sectional view of hypocenters for the 2017 Pohang earthquake sequence. (a) Spatial and temporal distribution of epicenters. The colors represent the timing of the seismic event after the mainshock (3 h, and 57, 167, and 340 days). Colors of the temporary seismic stations (squares) indicate stations installed on 10 November 2017 (red), between 15 and 18 November 2017 (blue), and after 19 February 2018 (yellow). (b) and (c) Hypocenters projected on cross-sections A–A' and B–B' (for the cross-section locations, see (a)). Modified from Kim et al. (2020). (For interpretation of the references to colour in this figure legend, the reader is referred to the web version of this article).

2. Geologic setting and Pohang enhanced geothermal system

The epicenter of the 2017 Pohang earthquake is located in the Pohang Basin (Kim et al., 2018a), which is a small-scale, early-middle Miocene sedimentary basin associated with the Cenozoic opening of the East Sea (or Japan Sea; Chough and Hwang, 1997; Yoon et al., 2014). The Pohang Basin consists of a kilometer-thick succession of Tertiary terrestrial to shallow-marine sedimentary rocks and pyroclastic/volcanic deposits (Sohn et al., 2001; Chough, 2013). NNW- to NNE-trending strike-slip faults and NNE- to NE-trending normal faults played an important role in the opening of the East Sea and the development of the Cenozoic basins (Son, 1998; Chough, 2013). Since the late Miocene, the area has been affected by a compressional stress regime, leading to the reactivation of some of the earlier transtensional strike-slip and normal faults as transpressional strike-slip and reverse faults, respectively (Ree et al., 2003; Park et al., 2006; Choi et al., 2012; Yoon et al., 2014).

Rocks in the Pohang EGS site comprise Permian granodiorite basement rocks intruded by gabbroic dikes (Lee et al., 2015; Yoon et al., 2015; Kim et al., 2018a). These rocks are unconformably overlain by a ~2400-m-thick succession of cover rocks (Lee et al., 2015). The cover rocks consist of Cretaceous sedimentary and volcanic rocks (~2000 m) that belong to a retro-arc basin (Gyeongsang Basin; Chough and Sohn, 2010), overlain by a relatively thin succession (200–400 m) of Tertiary sedimentary-pyroclastic rocks belonging to the Pohang Basin.

Drilling of injection and production wells in the Pohang EGS started in 2012 and finished in 2015 (Yoon et al., 2015). The drilling penetrated into the granodioritic basement, reaching depths of 4348 m and 4215 m for the vertical injection well (PX2) and the deviated production well (PX1), respectively (Kim et al., 2018a; Hofmann et al., 2019). At the surface, PX1 is positioned only 6 m from PX2, but at its bottom, they are

616 m apart (Hofmann et al., 2019). Five phases of hydraulic stimulation began in January 2016 with a maximum wellhead pressure of 89.2 MPa (maximum bottom-hole pressure of 131.8 MPa; Park et al., 2017). During the period of hydraulic stimulation, which continued until September 2017, the total and net injected fluid volumes were 12,798 m³ and 5841 m³, respectively (Kim et al., 2018a; Korean Government Commission, 2019). Each injection phase was followed, within a few days, by intense seismic activity. The Korean Government Commission on the Pohang earthquake found that a major fault existed between the bottoms of holes PX1 and PX2. The fault is characterized by a relatively thick (~4 m) impermeable gouge layer. Hole PX2 cuts through the fault at a depth of ca. 3800 m. The existence of this fault implies that a fluid barrier existed between the two wells (Korean Government Commission, 2019; Ellsworth et al., 2019). Thus, fluid injected along PX2 was injected directly (or near-directly) into the fault zone. Approximately two months after the final injection, the M_L 5.4 Pohang earthquake occurred at a depth of ~4.3 km (Kim et al., 2018a; Korean Government Commission, 2019). The earthquake was not associated with surface rupture, but significant surface deformation has been reported from Interferometric Synthetic Aperture Radar (InSAR) observations (Song and Lee, 2019) and a field survey (Choi et al., 2019). Estimated maximum and average displacements, based on the slip model of the InSAR data, were ~25 cm and ~15 cm, respectively (Song and Lee, 2019).

3. Aftershocks and rupture geometry

The deployment of eight temporary seismic stations around the EGS site five days before the mainshock generated data that provide constraints on the foreshocks, mainshock, and aftershocks of the Pohang earthquake. The number of seismic stations was increased to 13 after the

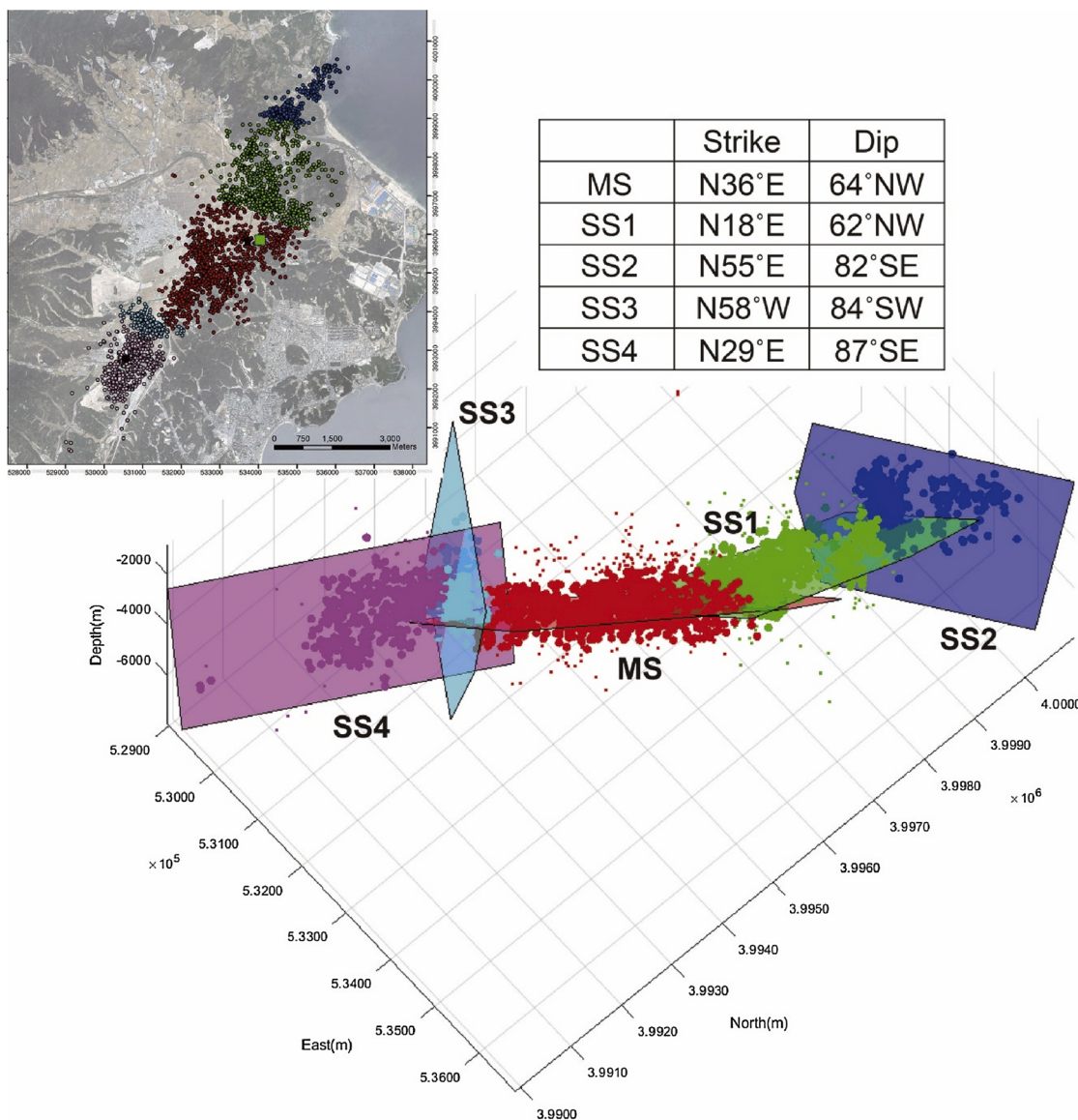


Fig. 2. 3-D distribution of hypocenters. Colored planes are best-fitting planes of hypocenters (large dots), representing the main segment (MS) and four subsidiary segments (SS1–SS4) of the earthquake rupture. Hypocenters that are >300 m away from the best-fitting planes (small dots) were excluded from the calculation. Inset: map of epicenters highlighting (in colors) the different segments (cf. Fig. 1a).

mainshock, and to 24 after the largest aftershock (M_L 4.6; see below) on 19 February 2018. This created an interstation spacing of <2 km around the mainshock epicenter and of <4 km on the periphery of the aftershock area (Fig. 1). From the seismic data, we detected a total of 3101 seismic events, including ten foreshocks, in the period from 10 November 2017 to 20 October 2018. Kim et al. (2018a) analyzed the first 3-h aftershocks using a 1-D velocity model (modified from Kim, 1999). We improved the earthquake locations by using an updated velocity model (Fig. S1) that was constrained by an active shot experiment at the Pohang EGS site (Korean Government Commission, 2019).

Most of the hypocenters of the Pohang earthquake sequence occurred at depths of 3–6 km (Fig. 1b and c). The initial rupture, based on seismic data obtained 3 h after the mainshock, occurred along a main segment (MS; N36°E/64°NW) ~3.5 km in length, and a subsidiary segment (SS1; N18°E/62°NW) that extends from the northeastern tip of the MS (Figs. 1 and 2). These rupture planes, calculated using MATLAB software, are best-fitting planes of hypocenters, excluding hypocenters that are located >300 m from the inferred planes (Fig. 2). Focal mechanism solutions of the 3-h seismicity indicate that MS and SS1 were

dominated by reverse and strike-slip kinematics, respectively (Kim et al., 2018a; Fig. 3). Following the initial 3-h period, subsequent seismic data show that a second subsidiary segment (SS2; N55°E/82°SE) propagated from the northern tip of SS1. The MS continued to rupture towards the southwest, extending ~1.4 km further than the initial (3-h) configuration. Subsequently, a third subsidiary segment (SS3; N58°W/84°SW), ~1.3 km in length, developed at the southwestern tip of and subperpendicular to the MS. A fourth subsidiary segment (SS4; N29°E/87°SE), ~1.9 km long, propagated southwestward from SS3 (Figs. 1 and 2). At a later stage of seismic activity (particularly 167–340 days after the mainshock), rupturing occurred mainly along the peripheries (or tips) of the rupture planes (Fig. 1 and video file in Supplementary data).

During the first 83 days after the mainshock, the frequency of aftershocks decreased with time, following Omori's law (Omori, 1894). Subsequently, a sudden surge of aftershocks associated with an M_L 4.6 event (11 February 2018) was followed again by an Omori's law decay in aftershock frequency (Fig. 4). The development of SS4 occurred simultaneously with the aftershock surge of the M_L 4.6 event (see video

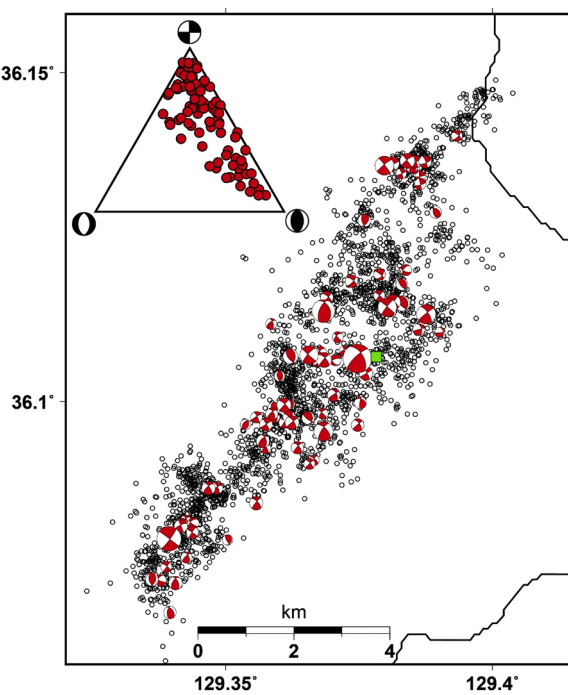


Fig. 3. Focal mechanism solutions of 94 largest earthquakes from the Pohang earthquake sequence. Inset: Ternary diagram of earthquake faulting mechanisms. Modified from Kim et al. (2020).

file in Supplementary data), thus implying that SS4 was an independent rupture.

An examination of the Coulomb stress change (ΔCF) using the program Coulomb 3 (Lin and Stein, 2004; Toda et al., 2005) allowed us to investigate whether the $M_L 4.6$ event was likely triggered by the MS. Coulomb 3 calculates changes in the static stress in response to the slip distribution of an earthquake and the likelihood that this change (ΔCF) would trigger an earthquake on a receiver fault. A positive value of ΔCF indicates that faulting is likely to occur on the receiver fault. The strike, dip, and rake of the receiver fault are chosen as one of the nodal planes, which is subparallel to the orientation of SS4. Our results show that ΔCF is positive around the southwestern and northeastern tips of the MS (Fig. 5). A spatial correlation between the hypocenter of the $M_L 4.6$ event and the southwestern (positive) zone indicates that the state of stress associated with the mainshock facilitated conditions for the $M_L 4.6$

event. Also, the MS tended to trigger more aftershocks in two opposite rupture tips.

4. Focal mechanism solutions

Focal mechanism solutions were calculated for 94 of the largest earthquakes from the Pohang earthquake sequence (Kim et al., 2020). For the solutions, we used the focal mechanism software HASH (Hardebeck and Shearer, 2002, 2003; <https://earthquake.usgs.gov/research/software/#HASH>) with P-wave first-motion polarities and S/P amplitude ratios (Kim et al., 2020). The results show reverse slip for the mainshock and strike-, reverse-, and oblique-slip faulting for the aftershocks. The lack of a normal-slip component indicates a contractional deformation regime (Fig. 3).

One of the nodal planes from the focal mechanism solution matches well with the relevant rupture plane obtained from the hypocentral distribution of the 2017 Pohang earthquake sequence in most cases (Figs. 6–10), although some nodal planes disagree with the average rupture plane. The disagreement implies that some aftershocks might occur on secondary fractures (or ruptures) rather than on the major rupture planes. The focal mechanism solutions of the events associated with the MS show mostly reverse or oblique-slip faulting and minor strike-slip faulting (Fig. 6). Focal plane mechanisms of all subsidiary segments are dominated by strike-slip or oblique-slip faulting (Figs. 7–10). In particular, all events associated with SS3 show strike-slip faulting (Fig. 9).

For stress inversion of the focal mechanism solutions, we used the STRESSINVERSE package (Vavryčuk, 2014; <https://www.ig.cas.cz/en/stress-inverse/>). The results show that the orientation of the maximum principal stress (σ_1) is $273^\circ/9^\circ$ (trend/plunge). The intermediate principal stress (σ_2) is subvertical (81°), indicating a strike-slip faulting regime (Fig. 11a). The bootstrapping analysis for the inverted stress field shows that the uncertainty of σ_1 is very low with the maximum error angle of about 3° . In contrast, the uncertainty of σ_2 and σ_3 (minimum principal stress) is relatively higher with the maximum error angle of about 34° . The stress ratio (R), $(\sigma_1 - \sigma_2)/(\sigma_1 - \sigma_3)$, is high (0.91 with a very low uncertainty of about 0.09; Fig. 11b), meaning that the magnitude of σ_2 is very similar to that of σ_3 (minimum principal stress) and that their permutation is highly likely. These alternations between vertical σ_2 and σ_3 are reflected in the evidence of reverse- oblique- and strike-slip faulting, as inferred from the focal mechanism solutions (Fig. 3). The relatively higher uncertainty of σ_2 and σ_3 orientations is partly due to the high value of the stress ratio (R).

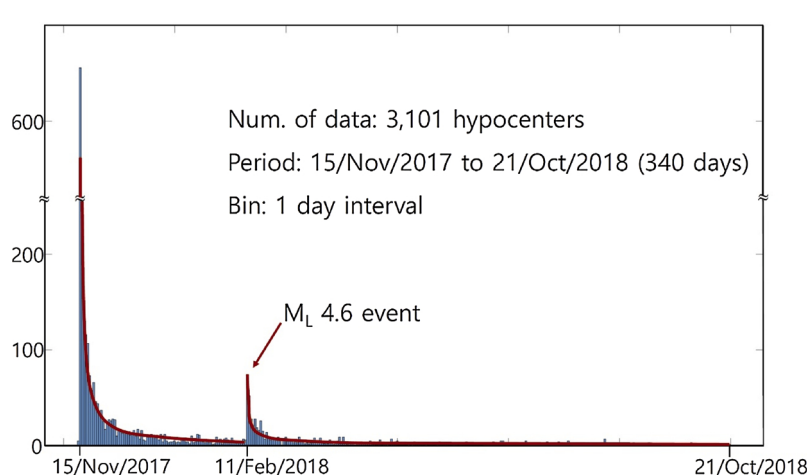


Fig. 4. Frequency diagram of the Pohang earthquakes. The aftershock sequence shows the Omori's law (red line) until 83 days after the mainshock, followed by another Omori's law decay. The Omori's lines are drawn by the method suggested by Tosi et al. (2010). (For interpretation of the references to colour in this figure legend, the reader is referred to the web version of this article).

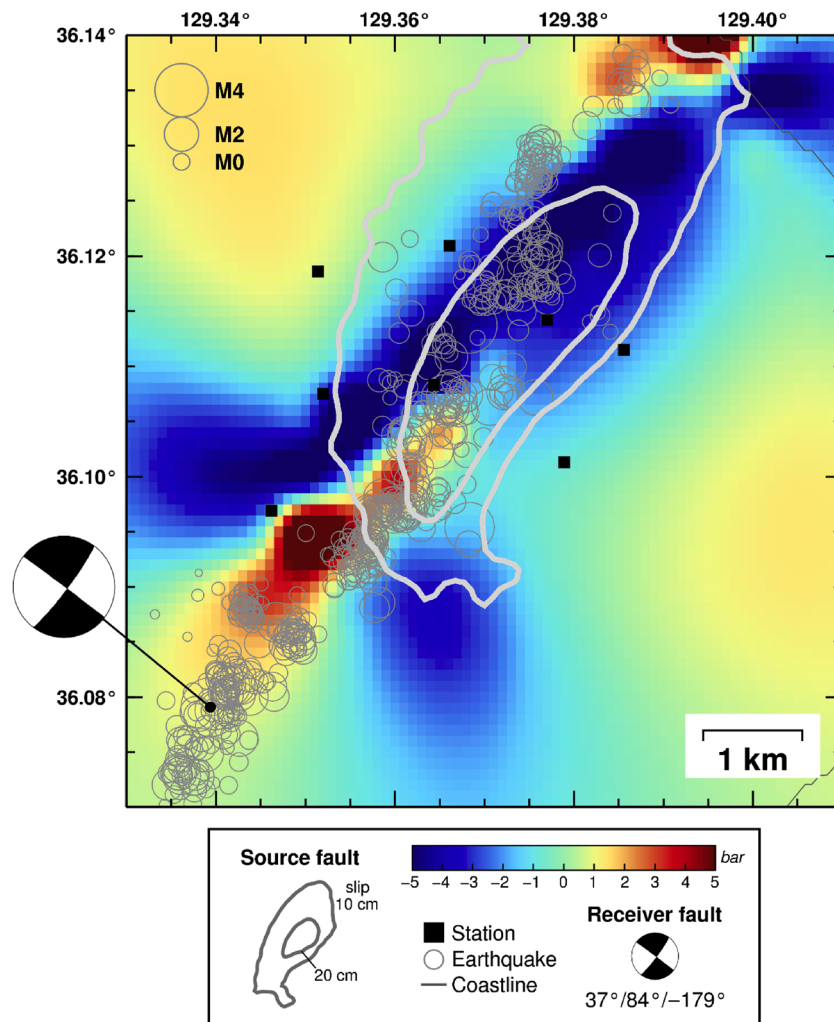


Fig. 5. Coulomb stress change in response to the mainshock. The calculation assumes that the subsidiary segment SS4 is the receiver fault. The slip distribution is from Song and Lee (2018). Epicenters are shown for aftershocks that occurred at depths of 5.1–5.5 km.

5. Slip tendency and reactivation of ruptures

Intracontinental earthquakes commonly reactivate pre-existing discontinuities rather than creating new faults (McKenzie, 1969; Sykes, 1978; Sibson, 1985). The generation of such earthquakes, therefore, is governed by the friction of the pre-existing discontinuities.

The slip tendency of a rupture plane is defined by the ratio between the shear stress and the normal stress that act on the rupture plane (Morris et al., 1996; Lisle and Srivastava, 2004). Factors controlling the slip tendency include the orientations of the rupture plane and principal stresses, the stress ratio, and the frictional coefficient (μ) of the rupture plane. For the orientation and stress ratio of the principal stresses, we used values calculated from stress inversion of the focal mechanism solutions described above. For the frictional coefficient, we considered two alternative values. First, we used the frictional coefficient value ($\mu = 0.85$) from Byerlee's law (Byerlee, 1978), assuming a lithostatic pressure of ~ 113 MPa at ~ 4.3 km (the hypocentral depth of the mainshock). Alternatively, 0.2 and 0.3 were chosen for frictional coefficient of chlorite gouge since the fault core of the causative fault from cuttings extracted from the PX-2 borehole consists of chlorite gouge (Korean Government Commission, 2019; T. Shimamoto, personal communication). Okamoto et al. (2019) have recently reported from friction experiments that the friction coefficient of chlorite gouge ranges from 0.2 to 0.3 at temperatures below 400 °C.

Stereographic projection can be used to visualize the reactivation

potential of rupture planes (Collettini and Trippetta, 2007). The background colors in these diagrams represent the slip tendency normalized by its maximum value ($0 \leq NTs \leq 1$). Fig. 12 shows that the average rupture planes of the MS, SS1, SS2, and SS3 are optimally oriented for reactivation, having normalized slip tendency values of 0.60–1.00 (Table 1). The highest normalized slip tendency value occurs on plane SS3. In contrast, under the current stress state, the average rupture plane of SS4 is misoriented for reactivation, as indicated by its relatively low normalized slip tendency value (Fig. 12 and Table 1). To reactive this plane, a high fluid pressure would be required.

Since the orientation of σ_2 and σ_3 determined from stress inversion of the focal mechanism solutions has some uncertainty (Fig. 11), we evaluated the uncertainty of slip tendency of the rupture planes reflecting that of the principal stress orientations. When we apply the new orientation of σ_2 and σ_3 with the maximum error (σ_2' and σ_3' in Fig. S2), the normalized slip tendency of MS and SS1 increases by 0.05–0.09, while that of SS2, SS3 and SS4 decreases by 0.01–0.12 (Table S1). Overall, the slip tendency of the rupture planes does not change much even with reflecting the maximum error of the principal stress orientations. When the magnitude of σ_3 is close to that of σ_2 (thus high R value), the shear stress of rupture planes is controlled mainly by the orientation σ_1 . Since the uncertainty of σ_1 orientation is negligible (Fig. 11), the uncertainty of σ_2 and σ_3 does not influence the slip tendency much.

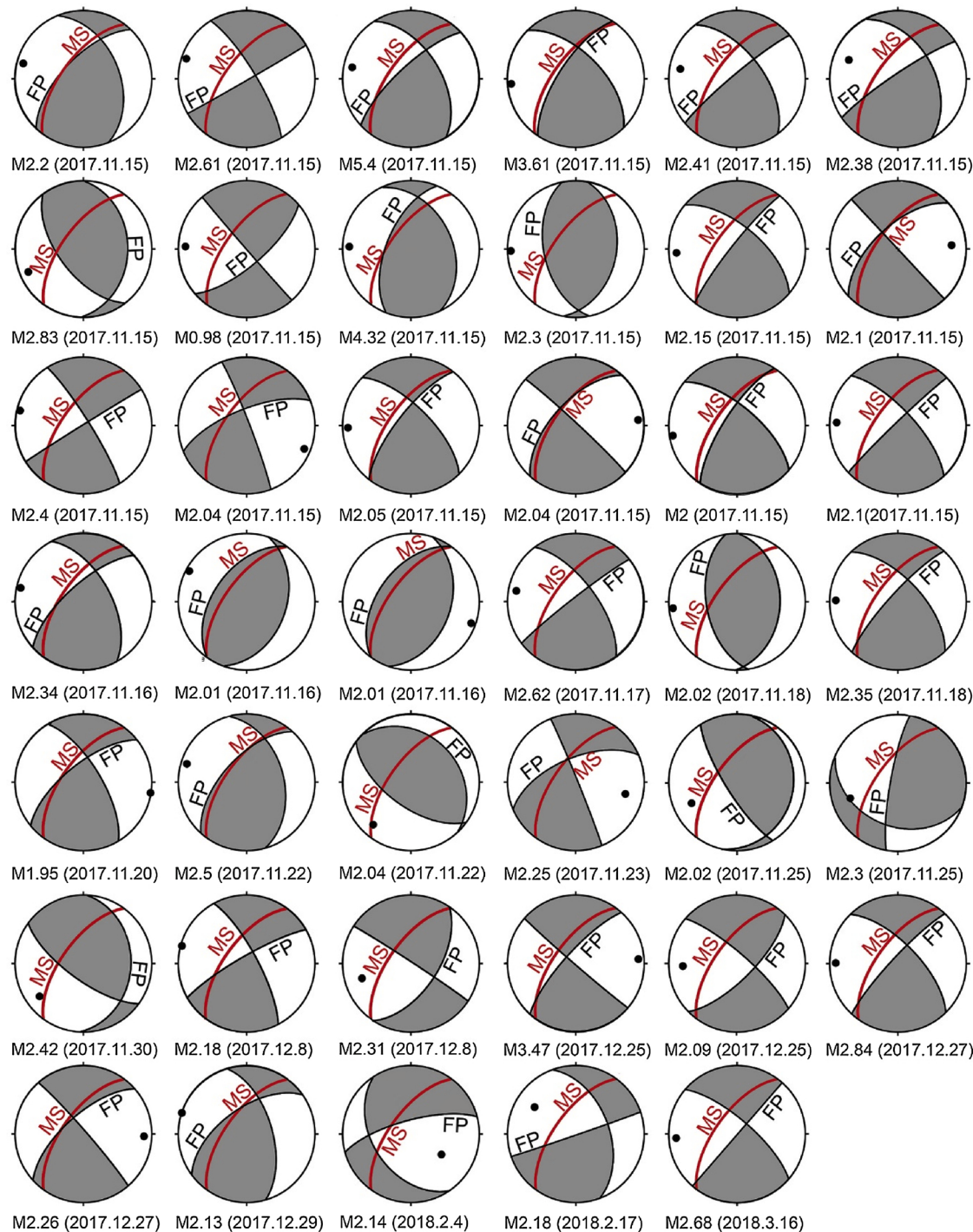


Fig. 6. Focal mechanism solutions for events belonging to the main segment (MS) of the Pohang earthquake rupture. The red great circle represents the best-fitting plane of the main segment. Black dot denotes compression axis. FP: fault plane. (For interpretation of the references to colour in this figure legend, the reader is referred to the web version of this article).

6. Discussion and conclusions

The Pohang earthquake sequence was accompanied by the reactivation of faults with complicated geometry (Fig. 2). On the basis of surface geology, geophysical data, and exploration drilling, it has been suggested that the Pohang Basin is underlain by subsurface fault structures (Song et al., 2015). The faults, according to Song et al. (2015), are either NNE- to NE-striking or E – W-striking normal faults that were developed (or reactivated) by extension during the Miocene. However, the fault geometry inferred from the aftershock distribution and focal

mechanism solutions of the Pohang earthquake sequence is more complex, showing one main segment (MS) and four subsidiary segments (SS1 to SS4). The stress perturbation caused by the mainshock, together with the frequency vs. time distribution of the aftershocks, indicates that the subsidiary rupture segment SS4 is an independent rupture plane that was triggered by the mainshock.

In southeastern Korea, the maximum principal stress direction (σ_1) is subhorizontal and oriented ENE (Chang et al., 2010; Soh et al., 2018). This principal stress direction is based on stress inversion of focal mechanism solutions, with characteristic focal depths of 10–20 km. The

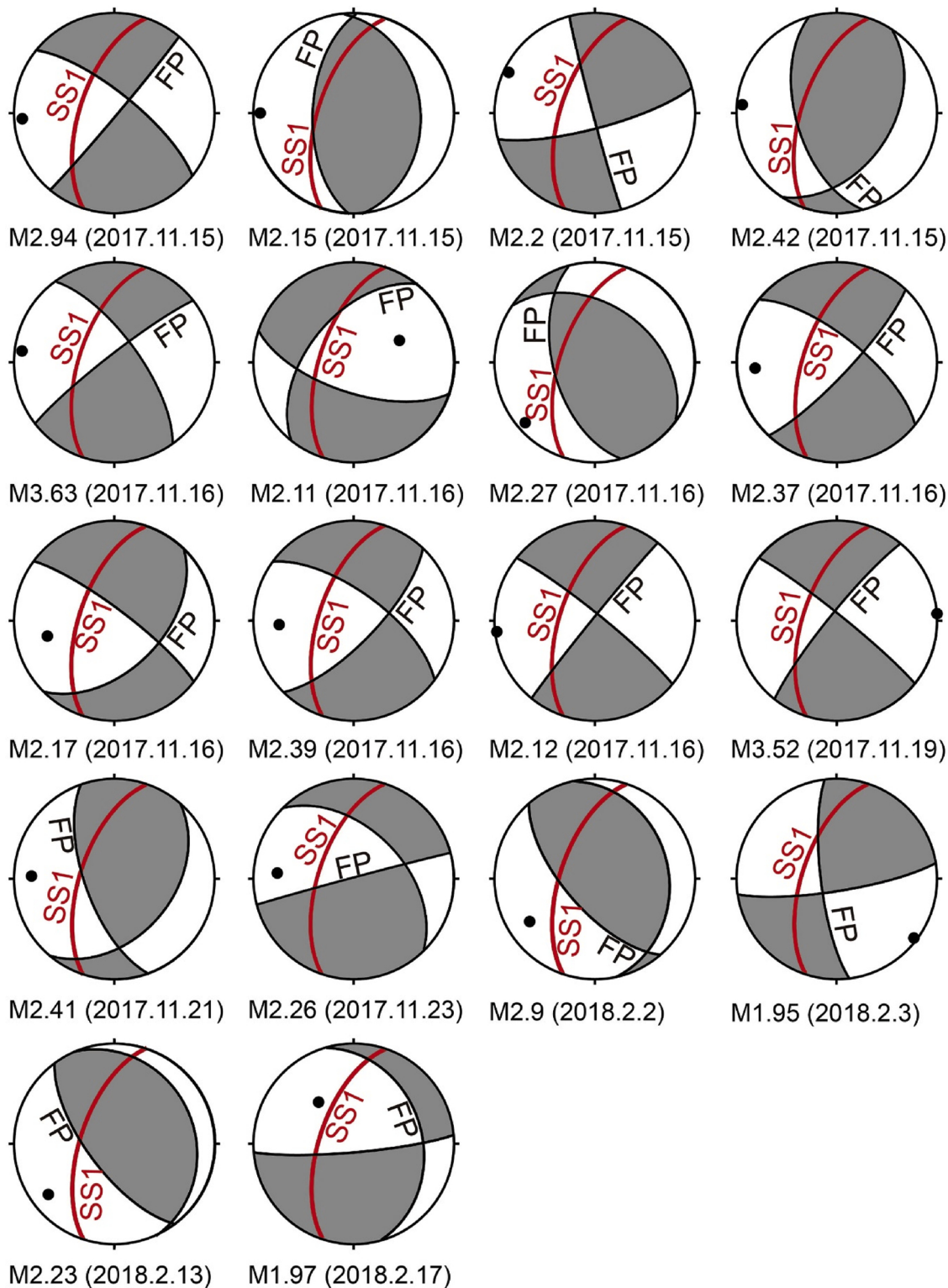


Fig. 7. Focal mechanism solutions for events belonging to the subsidiary segment, SS1. Explanation of the symbols is the same as that in Fig. 6.

orientation of σ_1 based on the shallower earthquakes (3–6 km) in Pohang is slightly different (subhorizontal E–W), implying that the orientation of the principal stress axes may change with depth. Indeed, the principal shortening direction in southeastern Korea is NW–SE, as indicated by present-day surface deformation calculated from geodetic data (Kim et al., 2018b), whereas the maximum principal stress deduced from borehole data (30–330 m depth) is highly variable. This variability in the orientations of the principal stresses might correspond to an

upward clockwise rotation of σ_1 .

At the focal depth of the Pohang earthquake sequence and the present-day stress orientation, all rupture planes except that of SS4 were optimally oriented for reactivation with all possible values of frictional coefficient. The reactivation of SS4, less favorably oriented than the other rupture planes, might have been facilitated with the stress perturbation by the mainshock and elevated pore pressure by migrating fluid. To evaluate the effect of migrating fluid, we estimated the hy-

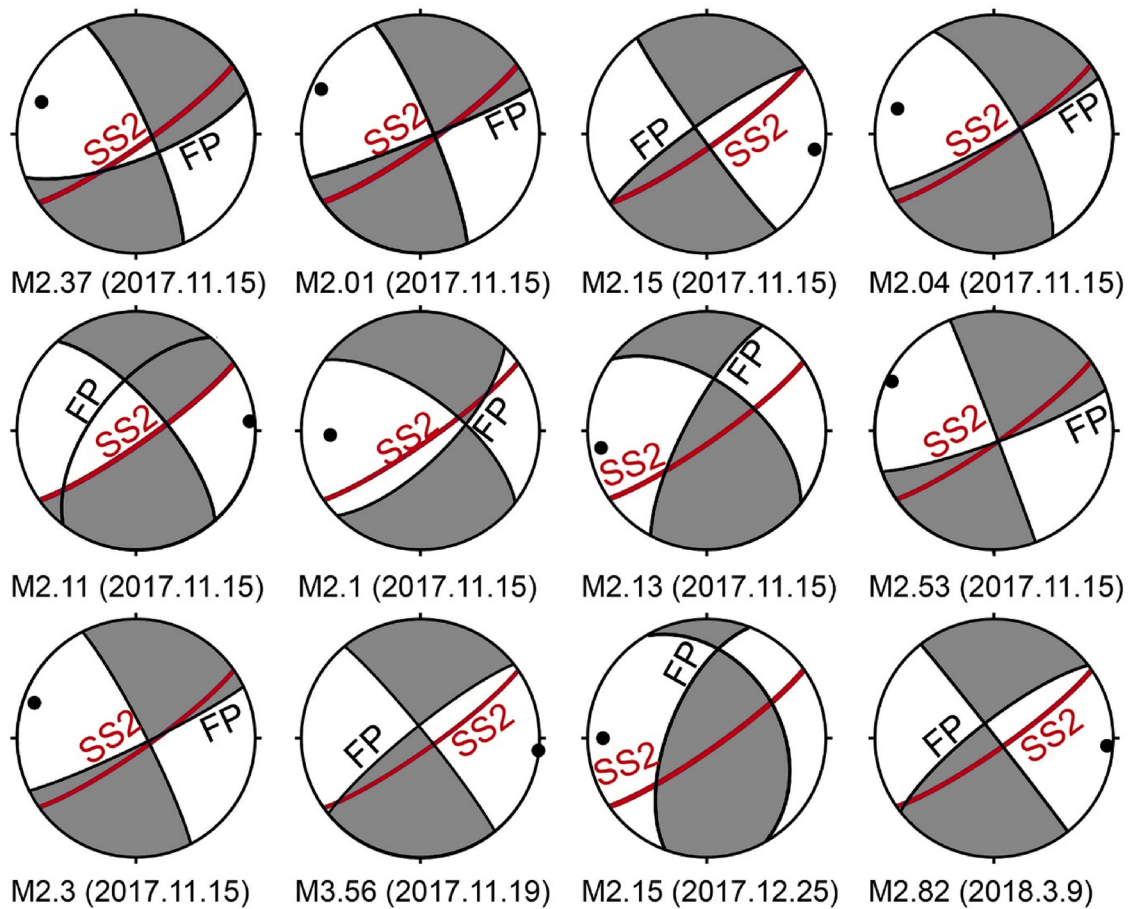


Fig. 8. Focal mechanism solutions for events belonging to the subsidiary segment, SS2. Explanation of the symbols is the same as that in Fig. 6.

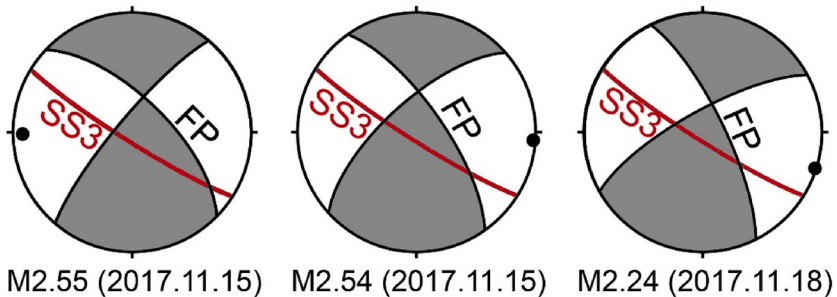


Fig. 9. Focal mechanism solutions for events belonging to the subsidiary segment, SS3. Explanation of the symbols is the same as that in Fig. 6.

draulic diffusivity from the earthquake migration pattern (Fig. S3; Shapiro et al., 1997). We calculated the distance between the well (PX-2) and the hypocenter (r), and compared it with the equation $r = \sqrt{4\pi Dt}$ where D is the hydraulic diffusivity and t is the time after the last injection (Fig. S3). The M_L 4.6 earthquake and its aftershocks lie within the curves, which of the D are $1 \times 10^{-1} \text{ m}^2/\text{s}$ and $2 \times 10^{-1} \text{ m}^2/\text{s}$. These values are larger than the previously estimated D for bedrock ($\sim 10^{-4} \text{ m}^2/\text{s}$; Lim et al., 2020), possibly implying that permeable fault might play a role as a conduit of the fluid.

The propagation of rupture planes more than 11 months after the mainshock seems unusual for a moderate-size earthquake. Despite significant surface deformation associated with the Pohang earthquake sequence, surface rupture has not been reported (Song and Lee, 2018; Choi et al., 2019). This suggests that a relatively large elastic strain was accumulated at the tips of the rupture planes. Accordingly, the increase

in static stress in response to the mainshock, possibly together with the influence of migrating fluids, allowed propagation of the rupture plane.

Finally, according to current theory on the relationship between the volume of injected fluid and earthquake magnitude, a substantially larger volume of fluid (>800 times the fluid volume injected at the Pohang EGS site) would be required to generate the M_w 5.5 earthquake at the Pohang EGS site (McGarr, 2014). Our study indicates that this condition can be relaxed if fluid is injected directly into an optimally oriented fault, thus inducing a larger earthquake than is predicted by theory.

CRediT authorship contribution statement

Jin-Han Ree: Conceptualization, Methodology, Writing - original draft, Writing - review & editing, Supervision, Funding acquisition.
Kwang-Hee Kim: Methodology, Validation, Formal analysis. **Hobin**

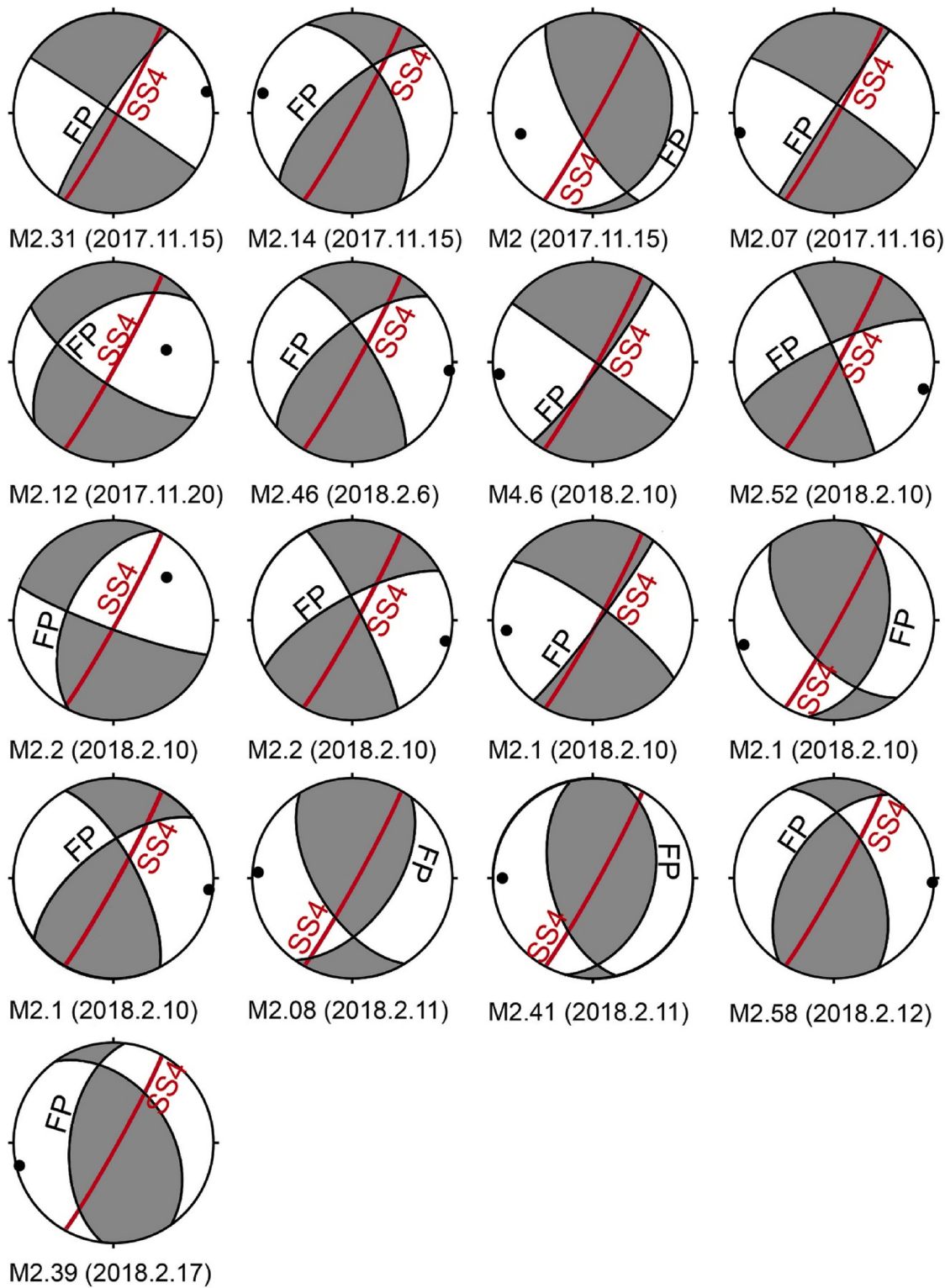


Fig. 10. Focal mechanism solutions for events belonging to the subsidiary segment, SS4. Explanation of the symbols is the same as that in Fig. 6.

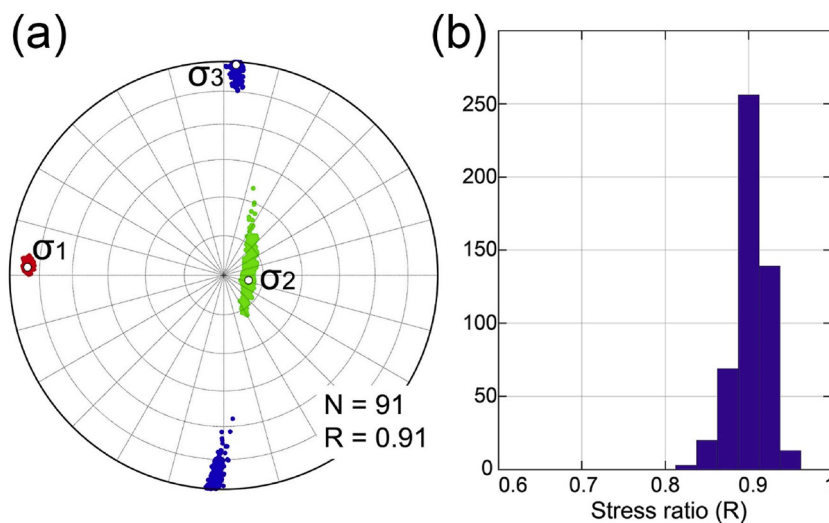


Fig. 11. (a) Orientation of principal stresses calculated from stress inversion of the focal mechanism solutions with 500 bootstrapping results. Stress ratio, $R = (\sigma_1 - \sigma_2)/(\sigma_1 - \sigma_3)$. N: number of focal mechanism solutions. (b) Histogram of stress ratio (R) with 500 bootstrapping results.

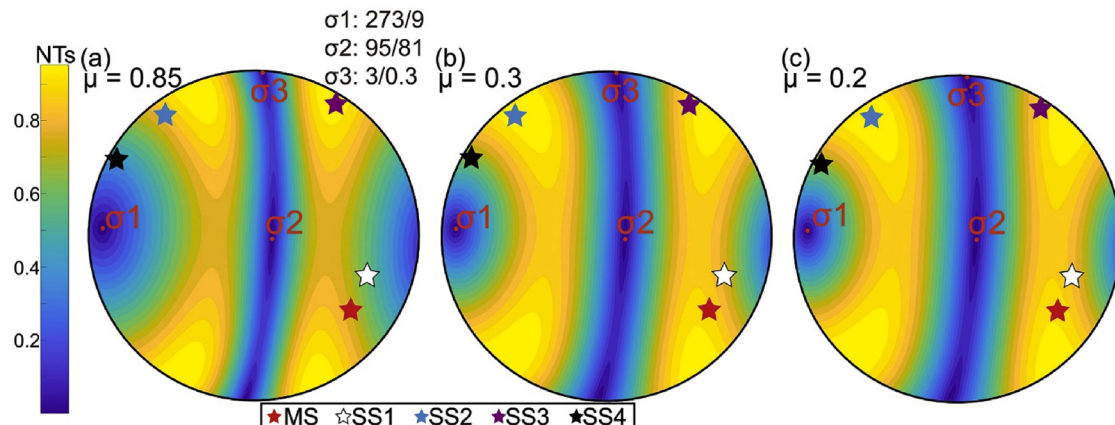


Fig. 12. Stereograms showing the slip tendency and the principal stresses associated with the Pohang earthquake sequence. Slip tendency for (a) a frictional coefficient (μ) = 0.6, (b) μ = 0.3 and (c) μ = 0.2. Background colors represent the value of normalized slip tendency ($0 \leq NTs \leq 1$).

Table 1

Normalized slip tendency (NTs) for each rupture segment with frictional coefficient (μ) of 0.85, 0.3 and 0.2.

	$\mu = 0.85$	$\mu = 0.3$	$\mu = 0.2$
MS	0.71	0.92	0.94
SS1	0.60	0.81	0.85
SS2	0.87	1.00	1.00
SS3	0.99	0.93	0.90
SS4	0.44	0.65	0.70

Lim: Conceptualization, Software, Formal analysis. **Wooseok Seo:** Data curation, Visualization. **Sungshil Kim:** Software, Formal analysis, Visualization. **Xiangyi An:** Software, Formal analysis, Visualization. **YoungHee Kim:** Methodology, Writing - review & editing.

Declaration of Competing Interest

The authors report no declarations of interest.

Acknowledgements

We thank two reviewers for their constructive comments that improved the earlier version of the manuscript. This work was supported by the Nuclear Safety Research Program through the Korea Foundation of Nuclear Safety (KoFONS) using financial resources granted by the Nuclear Safety and Security Commission (NSSC) of the Republic of Korea (No. 1705010).

Appendix A. Supplementary data

Supplementary material related to this article can be found, in the online version, at doi:<https://doi.org/10.1016/j.geothermics.2021.102048>.

References

- Byerlee, J.D., 1978. Friction of rocks. Pure Appl. Geophys. 116 (4–5), 615–626. <https://doi.org/10.1007/BF00876528>.
- Chang, C., Lee, J.B., Kang, T.S., 2010. Interaction between regional stress state and faults: complementary analysis of borehole in situ stress and earthquake focal

- mechanism in southeastern Korea. *Tectonophysics* 485 (1–4), 164–177. <https://doi.org/10.1016/j.tecto.2009.12.012>.
- Choi, H., Hong, T.K., He, X., Baag, C.E., 2012. Seismic evidence for reverse activation of a paleo-rifting system in the East Sea (Sea of Japan). *Tectonophysics* 572–573, 123–133. <https://doi.org/10.1016/j.tecto.2011.12.023>.
- Choi, J.H., Ko, K., Gihm, Y.S., Cho, C.S., Lee, H., Song, S.G., et al., 2019. Surface deformations and rupture processes associated with the 2017 Mw 5.4 Pohang, Korea, Earthquake. *Bull. Seismol. Soc. Am.* 109 (2), 756–769. <https://doi.org/10.1785/0120180167>.
- Chough, S.K., 2013. *Geology and Sedimentology of the Korean Peninsula*. Elsevier, London.
- Chough, S.K., Hwang, I.G., 1997. The Duksung fan delta, SE Korea: growth of delta lobes on a Gilbert-type topset in response to relative sea-level rise. *J. Sediment. Res.* 67 (4), 725–739. <https://doi.org/10.1306/D4268626-2B26-11D7-8648000102C1865D>.
- Chough, S.K., Sohn, Y.K., 2010. Tectonic and sedimentary evolution of a Cretaceous continental arc-backarc system in the Korean peninsula: new view. *Earth. Rev.* 101 (3–4), 225–249. <https://doi.org/10.1016/j.earscirev.2010.05.004>.
- Chung, T.W., Kim, W.H., 2000. Fault plane solutions for the June 26, 1997 Kyong-ju earthquake. *J. Korean Geophys. Soc.* 3 (4), 245–250 (in Korean with English abstract).
- Collettini, C., Trippetta, F., 2007. A slip tendency analysis to test mechanical and structural control on aftershock rupture planes. *Earth Planet. Sci. Lett.* 255 (3–4), 402–413. <https://doi.org/10.1016/j.epsl.2007.01.001>.
- Ellsworth, W.L., Giardini, D., Townsend, J., Ge, S., Shimamoto, T., 2019. Triggering of the Pohang, Korea, earthquake (Mw 5.5) by enhanced geothermal system stimulation. *Seismol. Res. Lett.* 90 (5), 1844–1858. <https://doi.org/10.1785/0220190102>.
- Grigoli, F., Cesca, S., Rinaldi, A.P., Manconi, A., López-Comino, J.A., Clinton, J.F., et al., 2018. The November 2017 M w 5.5 Pohang earthquake: a possible case of induced seismicity in South Korea. *Science* 360 (6392), 1003–1006. <https://doi.org/10.1126/science.aat2010>.
- Hardebeck, J., Shearer, P.M., 2002. A New method for determining first-motion focal mechanisms. *Bull. Seismol. Soc. Am.* 92 (6), 2264–2276. <https://doi.org/10.1785/0120010200>.
- Hardebeck, J., Shearer, P.M., 2003. Using S/P Amplitude ratios to constrain the focal mechanisms of small earthquakes. *Bull. Seismol. Soc. Am.* 93 (6), 2434–2444. <https://doi.org/10.1785/0120020236>.
- Hofmann, H., Zimmermann, G., Farkas, M., Huenges, E., Zang, A., Leonhardt, M., et al., 2019. First field application of cyclic soft stimulation at the Pohang Enhanced Geothermal System site in Korea. *Geophys. J. Int.* 217 (2), 926–949. <https://doi.org/10.1093/gji/ggz058>.
- Kim, W., 1999. P-wave velocity structure of upper crust in the vicinity of the Yangsan Fault region. *Geosci. J.* 3 (1), 17–22. <https://doi.org/10.1007/BF02910230>.
- Kim, K.H., Kang, T.S., Rhee, J., Kim, Y.H., Park, Y., Kang, S., et al., 2016. The 12 September 2016 Gyeongju earthquakes: 2. Temporary seismic network for monitoring aftershocks. *Geosci. J.* 20 (6), 753–757. <https://doi.org/10.1007/s12303-016-0034-9>.
- Kim, K.H., Ree, J.H., Kim, Y., Kim, S., Kang, S.Y., Seo, W., 2018a. Assessing whether the 2017 M w 5.4 Pohang earthquake in South Korea was an induced event. *Science* 360 (6392), 1007–1009. <https://doi.org/10.1126/science.aat6081>.
- Kim, S., Ree, J.H., Yoon, H.S., Choi, B.K., Park, P.H., 2018b. Crustal deformation of South Korea after the Tohoku-Oki earthquake: deformation heterogeneity and seismic activity. *Tectonics* 37 (8), 2389–2403. <https://doi.org/10.1029/2018TC004967>.
- Kim, K.H., Seo, W., Han, J., Kwon, J., Kang, S.Y., Ree, J.H., Kim, S., Liu, K., 2020. The 2017 M₁ 5.4 Pohang earthquake sequence, Korea, recorded by a dense seismic network. *Tectonophysics*. <https://doi.org/10.1016/j.tecto.2019.228306> (in press).
- Korean Government Commission, 2019. Summary Report of the Korean Government Commission on Relations Between the 2017 Pohang Earthquake and EGS Project. Geological Society of Korea, Seoul, South Korea. <https://doi.org/10.22719/KETEP-20183010111860>.
- Lee, K., Kim, K.H., Chang, T.W., 1986. Seismicity of the Korean Peninsula (II): seismicity of the northern part of the Yangsan Fault. *J. Geol. Soc. Korea* 22 (4), 347–365.
- Lee, T.J., Song, Y., Park, D.W., Jeon, J., Yoon, W.S., 2015. Three dimensional geological model of Pohang EGS Pilot Site, Korea. *World Geotherm. Congress* 2015 (April), 6.
- Lee, K.K., Ellsworth, W.L., Giardini, D., Townsend, J., Ge, S., Shimamoto, T., Yeo, I.W., Kang, T.S., Rhee, J., Sheen, D.H., et al., 2019. Managing injection-induced seismic risks. *Science* 364 (6442), 730–732. <https://doi.org/10.1126/science.aax1878>.
- Lim, H., Deng, K., Kim, Y.H., Ree, J.-H., Song, T., -R, A., Kim, K.-H., 2020. The 2017 Mw 5.5 Pohang Earthquake, South Korea, and Poroelastic stress changes associated with fluid injection. *J. Geophys. Res. Solid Earth* 125 (6), 1–18. <https://doi.org/10.1029/2019JB019134>.
- Lin, J., Stein, R.S., 2004. Stress triggering in thrust and subduction earthquakes, and stress interaction between the southern San Andreas and nearby thrust and strike-slip faults. *J. Geophys. Res. Solid Earth* 109 (2), B02303. <https://doi.org/10.1029/2003JB002607>.
- Lisle, R., Srivastava, D.C., 2004. Test of frictional reactivation theory for faults and validity of fault-slip analysis. *Geology* 32 (7), 569–572. <https://doi.org/10.1130/G24048.1>.
- McGarr, A., 2014. Maximum magnitude earthquakes induced by fluid injection. *J. Geophys. Res. Solid Earth* 119 (2), 1008–1019. <https://doi.org/10.1002/2013JB010597>.
- McKenzie, D.P., 1969. Relation between fault plane solutions for earthquakes and directions of principal stresses. *Bull. Seismol. Soc. Am.* 59 (2), 591–601.
- Morris, A., Ferrill, D.A., Henderson, D.B., 1996. Slip-tendency analysis and fault reactivation. *Geology* 24 (3), 275–278. [https://doi.org/10.1130/0091-7613\(1996\)024<0275:STAAGR>2.3.CO;2](https://doi.org/10.1130/0091-7613(1996)024<0275:STAAGR>2.3.CO;2).
- Okamoto, A.S., Verberne, B.A., Niemeijer, A.R., Takahashi, M., Shimizu, I., Ueda, T., Spiers, C.J., 2019. Frictional properties of simulated chlorite gouge at hydrothermal conditions: implications for subduction megathrusts. *J. Geophys. Res. Solid Earth* 124 (5), 4545–4565. <https://doi.org/10.1029/2018JB017205>.
- Omori, F., 1894. On the aftershocks of earthquakes. *J. Coll. Sci. T.* 7, 111–200. Imperial University of Tokyo.
- Park, Y., Ree, J.H., Yoo, S.H., 2006. Fault slip analysis of Quaternary faults in southeastern Korea. *Gondwana Res.* 9 (1–2), 118–125. <https://doi.org/10.1016/j.gr.2005.06.007>.
- Park, S., Xie, L., Kim, K.I., Kwon, S., Min, K.B., Choi, J., et al., 2017. First hydraulic stimulation in fractured geothermal reservoir in Pohang PX-2 well. *Procedia Eng.* 191, 829–837. <https://doi.org/10.1016/j.proeng.2017.05.250>.
- Ree, J.H., Lee, Y.J., Rhodes, E.J., Park, Y., Kwon, S.T., Chwae, U., Jeon, J.S., Lee, B., 2003. Quaternary reactivation of Tertiary faults in the southeastern Korean Peninsula: age constraint by optically stimulated luminescence dating. *Isl. Arc* 12 (1), 1–12. <https://doi.org/10.1046/j.1440-1738.2003.00372.x>.
- Shapiro, S.A., Huenges, E., Borm, G., 1997. Estimating the crust permeability from fluid-injection-induced seismic emission at the KTB site. *Geophys. J. Int.* 131 (2), F15–F18. <https://doi.org/10.1111/j.1365-246X.1997.tb01215.x>.
- Sibson, R.H., 1985. A note on fault reactivation. *J. Struct. Geol.* 7 (6), 751–754. [https://doi.org/10.1016/0191-8141\(85\)90150-6](https://doi.org/10.1016/0191-8141(85)90150-6).
- Sohn, I., Chang, C., Lee, J., Hong, T., Park, E.S., 2018. Tectonic stress orientations and magnitudes, and friction of faults, deduced from earthquake focal mechanism inversions over the Korean Peninsula. *Geophys. J. Int.* 213 (2), 1360–1373. <https://doi.org/10.1093/gji/ggy061>.
- Sohn, Y.K., Rhee, C.W., Shon, H., 2001. Revised stratigraphy and reinterpretation of the Miocene Pohang basinfill, SE Korea: sequence development in response to tectonism and eustasy in a back-arc basin margin. *Sediment. Geol.* 143 (3–4), 265–285. [https://doi.org/10.1016/S0037-0738\(01\)00100-2](https://doi.org/10.1016/S0037-0738(01)00100-2).
- Son, M., 1998. Formation and Evolution of the Tertiary Miocene Basins in Southeastern Korea: Structural and Paleomagnetic Approaches. Pusan National University, Pusan.
- Song, S.G., Lee, H., 2018. Static slip model of the 2017 Mw 5.4 Pohang, South Korea, earthquake, constrained by InSAR data. *Seismol. Res. Lett.* 90 (1), 140–148. <https://doi.org/10.1785/0220180156>.
- Song, C.W., Son, M., Sohn, Y.K., Han, R., Shinn, Y.J., Kim, J.C., 2015. A study on potential geologic facility sites for carbon dioxide storage in the Miocene Pohang Basin, SE Korea. *J. Geol. Soc. Korea* 51 (1), 53–66. <https://doi.org/10.14770/jgsk.2015.51.1.53> (in Korean with English abstract).
- Sykes, L.R., 1978. Intraplate seismicity, reactivation of preexisting zones of weakness, alkaline magmatism, and other tectonism postdating continental fragmentation. *Rev. Geophys. Space Phys.* 16, 621–687. <https://doi.org/10.1029/RG016i004p00621>.
- Toda, S., Stein, R.S., Richards-Dinger, K., Bozkurt, S., 2005. Forecasting the evolution of seismicity in southern California: animations built on earthquake stress transfer. *J. Geophys. Res. Solid Earth* 110 (5), B05S16. <https://doi.org/10.1029/2004JB003415>.
- Tosi, P., de Rubeis, V., Sbarra, P., 2010. Stacked analysis of earthquake sequences: statistical space-time definition of clustering and Omori law behavior. In: de Rubeis, V., Czechowski, Z., Teissseyre, R. (Eds.), *Synchronization and Triggering: from Fracture to Earthquake Processes*, GeoPlanet: Earth and Planetary Sciences. Springer-Verlag, Berlin, pp. 323–337. https://doi.org/10.1007/978-3-642-12300-9_19.
- Vavryčuk, V., 2014. Iterative joint inversion for stress and fault orientations from focal mechanisms. *Geophys. J. Int.* 199 (1), 69–77. <https://doi.org/10.1093/gji/ggu224>.
- Yoon, S.H., Sohn, Y.K., Chough, S.K., 2014. Tectonic, sedimentary, and volcanic evolution of a back-arc basin in the East Sea (Sea of Japan). *Mar. Geol.* 352, 70–88. <https://doi.org/10.1016/j.margeo.2014.03.004>.
- Yoon, K.S., Jeon, J.S., Hong, H.K., Kim, H.G., Hakan, A., Park, J.H., Yoon, W.S., 2015. Deep drilling experience for Pohang enhanced geothermal project in Korea. *World Geotherm. Congress* 2015 (April), 6.